Profiling the initial burst of beneficial genetic diversity in clonal cell populations to anticipate evolution

Daniel E. Deatherage and Jeffrey E. Barrick*

Department of Molecular Biosciences, Center for Systems and Synthetic Biology,

The University of Texas at Austin, Austin, Texas 78712, U.S.A.

* Email: jbarrick@cm.utexas.edu

Data Availability Statement: DNA sequence files are available from the NCBI Sequence Read Archive (accession number PRJNA601748). Code and processed data files are available on GitHub (https://github.com/barricklab/adaptome-capture).

Funding: This work was supported by the Cancer Prevention & Research Institute of Texas (CPRIT) (RP130124), the National Institutes of Health (R00-GM087550), the National Science Foundation (CBET-1554179 and DEB-1813069), and the NSF BEACON Center for the Study of Evolution in Action (DBI-0939454). D.E.D. acknowledges support from a University of Texas at Austin CPRIT research traineeship (RP101501). The funders had no role in study design, data collection and analysis, decision to publish, or preparation of the manuscript.

Competing interests: J.E.B. is the owner of Evolvomics LLC. D.E.D. has been a paid consultant for Evolvomics LLC.

Abstract

Clonal populations of cells continuously evolve new genetic diversity, but it takes a significant amount of time for the progeny of a single cell with a new beneficial mutation to outstrip both its ancestor and competitors to fully dominate a population. If these driver mutations can be discovered earlier—while they are still extremely rare—and profiled in large numbers, it may be possible to anticipate the future evolution of similar cell populations. For example, one could diagnose the likely course of incipient diseases, such as cancer and bacterial infections, and better judge which treatments will be effective, by tracking rare drug-resistant variants. To test this approach, we replayed the first 500 generations of a >70,000-generation *Escherichia coli* experiment and examined the trajectories of new mutations in eight genes known to be under positive selection in this environment in six populations. By employing a deep sequencing procedure using unique molecular identifiers and target enrichment we were able to track 301 beneficial mutations at frequencies as low as 0.01% and infer the fitness effects of 240 of these. Distinct molecular signatures of selection on protein structure and function were evident for the three genes in which beneficial mutations were most common (*nadR*, *pykF*, and *topA*). We detected mutations hundreds of generations before they became dominant and tracked beneficial alleles in genes that were not mutated in the long-term experiment until thousands of generations had passed. This type of targeted adaptome sequencing approach could function as an early warning system to inform interventions that aim to prevent undesirable evolution.

43 **Introduction**

44 New genetic variation naturally arises in lineages of cells and organisms during genome
45 replication and repair. These *de novo* mutations are the main drivers of adaptive evolution in
46 many populations, particularly those with little or no recombination or standing genetic variation.
47 In large laboratory populations of asexual microbes, numerous lineages with different beneficial
48 mutations arise and contend within a population before any one outcompetes the ancestor and its
49 competitors (Good et al., 2017; Lang et al., 2013; Maddamsetti et al., 2015). This 'clonal
50 interference' leads to heterogeneous populations with many lineages simultaneously adapting via
51 distinct sets of mutations, though often these mutations are in a small subset of genes that are
52 under the strongest selection (Desai et al., 2012; Gerrish and Lenski, 1998; Park and Krug,
53 2007).

54 In human cancers and chronic microbial infections, single cells clonally expand in a similar
55 fashion by evolving driver mutations that lead to disease progression and drug resistance. Both
56 solid tumors and blood cancers have been shown to be genetically heterogeneous (Marusyk et
57 al., 2012; Merlo et al., 2006; Thomas et al., 2006). *De novo* mutations taking over normal cell
58 populations can lead to carcinogenesis (Genovese et al., 2014; Watson et al., 2020), and
59 mutations in cancer cells drive neoplastic progression (Merlo et al., 2010), differences in
60 responses to chemotherapy (Landau et al., 2013), and relapse (Ding et al., 2012). Populations of
61 *Pseudomonas aeruginosa* and other bacteria that persistently infect the lungs of cystic fibrosis
62 patients become increasingly invasive and antibiotic resistant over time (Marvig et al., 2015;
63 Stefani et al., 2017; Winstanley et al., 2016). In these cases, there are also specific genetic loci
64 that are repeatedly mutated in different individuals. Better predicting the future evolution of each

65 of these types of cell populations and others would inform treatment decisions and improve
66 medical outcomes.
67 Cells used in biomanufacturing are also prone to evolving unwanted genetic heterogeneity
68 (Renda et al., 2014; Rugbjerg and Sommer, 2019). Typically, these cells have been heavily
69 engineered to optimize the titer of a product of interest at the expense of rapid cellular replication
70 (Lee and Kim, 2015; Nielsen and Keasling, 2016). Therefore, there are strong selective pressures
71 for 'escape mutations' that cause production to decline. Usually escape mutations directly
72 inactivate one or more key genes in the engineered pathway. The resulting nonproducing cells
73 can become dominant during the many cell divisions that are necessary to scale these processes
74 up to large bioreactors (Rugbjerg et al., 2018; Sandoval et al., 2014; Zelder and Hauer, 2000).
75 The ability to predict the future evolution of nonproducing cells before attempting scale-up could
76 guide strain design decisions and thereby improve the efficiency of industrial processes.
77 Evolution experiments conducted in laboratory environments reproduce key aspects of
78 microbial evolution that are observed in chronic infections and bioreactors (Barrick and Lenski,
79 2013; Gresham and Dunham, 2014). Certain aspects of genomic and phenotypic evolution in
80 these systems are surprisingly predictable while others are not (Barrick, 2020; Cvijović et al.,
81 2018; Furusawa et al., 2018; McDonald, 2019; Rainey et al., 2017). In theory, profiling many
82 rare mutations in the earliest stages of clonal interference using high-throughput DNA
83 sequencing should allow one to anticipate the future evolution of a population and other
84 populations that evolve in similar environments. Existing studies have generally been limited to
85 reliably identifying mutations that are present in at least one sample at a frequency above ~1-
86 10% (due to sequencing depth costs and per-base error rates) when they have already succeeded
87 in becoming dominant (Barrick and Lenski, 2009; Chubiz et al., 2012; Good et al., 2017; Lang et

88 al., 2013; Traverse et al., 2013). Theory and simulations predict that many more highly
89 beneficial mutations evolve in these populations but never reach such high frequencies before
90 they are driven extinct (Desai et al., 2012; Gerrish and Lenski, 1998), and recent studies that
91 track the evolution of barcoded lineages of microbes show that this is the case (Levy et al., 2015;
92 Venkataram et al., 2016).

93 Here, we used methods for selectively increasing sequencing depth and lowering sequencing
94 error rates to deeply profile the initial burst of rare beneficial mutations in laboratory populations
95 of *E. coli*. We directly identified diverse beneficial mutations in eight genes when they were
96 orders of magnitude lower in frequency and hundreds of generations earlier than could be
97 accomplished by standard metagenomic sequencing methods. Molecular signatures in the large
98 sets of beneficial mutations found in three of these genes made it possible to understand the
99 nature of selection acting on their functions in this environment. By comparing our results to the
100 long history of a >70,000-generation *E. coli* evolution experiment that used the same ancestral
101 strains and nearly identical culture conditions (Lenski et al., 1991), we are able to evaluate the
102 potential of this type of targeted adaptome analysis for anticipating the evolution of cell
103 populations.

104

105 ## Results

106 **Replaying the beginning of a long-term evolution experiment**

107 We initially examined the evolution of nine replicate *E. coli* populations that were propagated
108 via daily serial transfers in glucose-limited minimal medium for 500 generations. Our
109 experiment used the same *E. coli* strains as the Lenski long-term evolution experiment (LTEE)
110 and similar growth conditions (see **Methods**). Each population was inoculated with a 50/50

111 mixture of the two neutrally marked LTEE ancestor strains to visualize the initial selective sweep
112 (Hegreness et al., 2006). Most populations maintained a roughly equal representation of
113 descendants of both ancestral strains through the first 300 generations (**Fig. 1**). These dynamics
114 are in agreement with what has previously been observed in studies of the LTEE, where few
115 mutations reach a high frequency in the first few hundred generations of evolution (Good et al.,
116 2017). We did not further analyze three populations. Two of these (A4 and A5) were
117 purposefully omitted because they exhibited early sweeps of one marker type, which indicates
118 that their dynamics might have been dominated by one or a few "jackpot" mutations that
119 occurred very early during outgrowth of these populations from single cells. The third omitted
120 population (A8) exhibited typical marker dynamics.
121

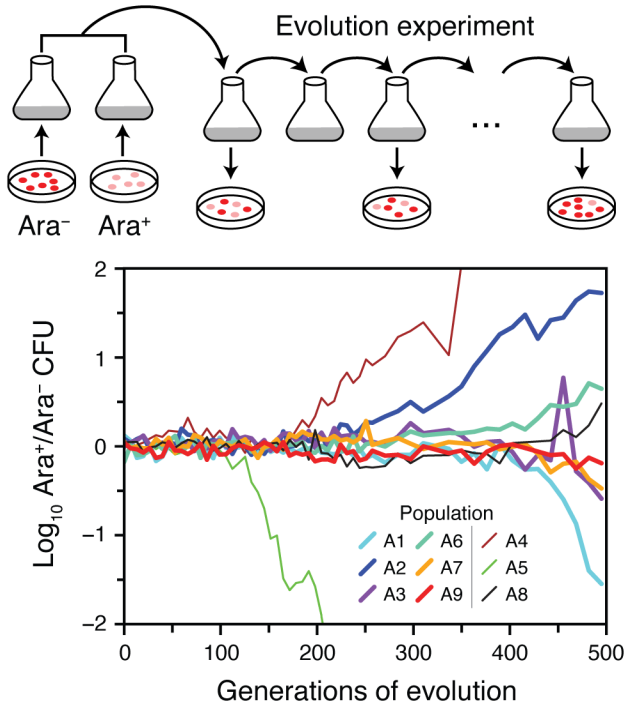

122

123 **Figure 1. Replaying the first selective sweep of a long-term evolution experiment.** Nine *E.*
124 *coli* populations were initiated from equal mixtures of two variants of the ancestral strain that
125 differ in a neutral genetic marker for arabinose utilization (Ara). We observed the evolutionary
126 dynamics of these populations over ~500 generations of regrowth from 75 daily 1:100 serial

127 transfers by periodically plating dilutions of each population on indicator agar. The ratio of Ara^+
128 cells (pink colonies) to Ara^- cells (red colonies) diverges from 1:1 when descendants of one
129 ancestor type accumulate enough of a fitness advantage due to *de novo* beneficial mutations that
130 they take over. We focused further analysis on six of the nine populations (thick lines).
131

132 **Reconstructing the trajectories of new beneficial mutations**

133 We next performed deep sequencing of eight genes at ~25 generation increments over the entire
134 500 generations of the evolution experiment for four of the six populations that we examined
135 further. These eight genes (*nadR*, *pykF*, *topA*, *spoT*, *fabR*, *ybaL*, *hslU*, and *iclR*) are known to be
136 targets of selection in the LTEE (Good et al., 2017; Tenaillon et al., 2016). Illumina libraries
137 containing unique molecular identifiers (Schmitt et al., 2012) were prepared for sequencing and
138 enriched for the regions of interest using solution based hybridization (Bainbridge et al., 2010).
139 Consensus sequence reads were generated based on groups of reads with identical unique
140 molecular identifiers and aligned to the *E. coli* genome to predict mutations, including using
141 split-read mapping to identify transposon insertions and large deletions (**Fig. 2A**). The
142 enrichment procedure was effective: an average of 73.5% of consensus reads per sample mapped
143 to the targeted regions that together constitute only 0.780% of the 4.63 Mbp genome. In the
144 sample with the median number of total consensus reads, the average coverage depth across each
145 of the eight genes of interest exceeded 5,000 (**Fig. 2B**). After analyzing patterns in mutation
146 frequencies over time to eliminate other systematic biases (see Methods), we were able to track
147 the evolution and competition of 181 *de novo* mutations, including when many were present in
148 less than 0.1% of the cells in a population (**Fig. 2C**, **Fig. 3**).

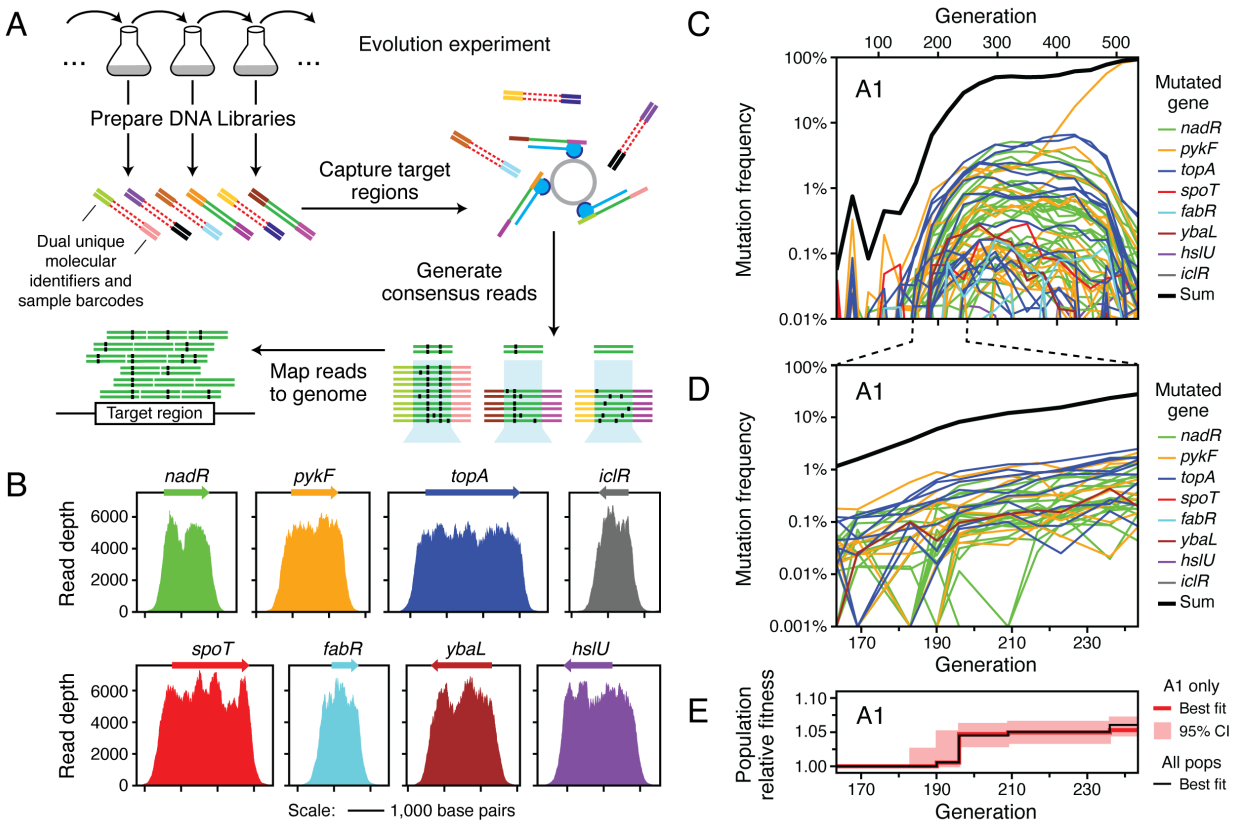

Figure 2. Profiling many beneficial mutations in the first selective sweep by deep sequencing. (A) Schematic of the deep sequencing approach. Genomic DNA is directly isolated from the *E. coli* populations and prepared for paired-end Illumina sequencing with sample barcodes and dual unique molecular identifiers (colored ends attached to red/green double stranded DNA). DNA fragments matching the targeted genome regions (green centers) are captured by probes (blue) bound to magnetic beads and other sequences are washed away (red centers). Reads in pairs that have the same dual unique molecular identifiers, which implies that they were PCR amplified during library preparation from the same original genomic DNA fragment, are used to construct consensus reads to eliminate sequencing errors. Consensus reads are mapped to the reference genome to call sequence variants. (B) Enrichment of reads mapping to eight genes known to be early targets of selection in this environment from the long-term evolution experiment. The final coverage depth of consensus reads in and around these genes is shown for a typical sample (population A7 at 500 generations). (C) Frequency trajectories for mutations in the eight targeted genes as well as the sum total frequency in population A1 over the complete time course of the evolution experiment. When a mutation was not detected at a time point, its trajectory is shown as passing through a frequency of 0.0001% (outside of the plot bounds). (D) Mutation frequency trajectories for population A1 during the window from 133 to 213 generations when mutations were first reaching detectable frequencies as they outcompeted the ancestral genotype. At time points when a mutation was not detected, its frequency is shown as 0.001% (at the bottom of the plot). (E) Estimated relative fitness of population A1 in each interval between the time points in the window time course. The frequency trajectories of all beneficial mutations in the initial sweep shown in D were used to jointly estimate the average fitness of the entire population from the deceleration in the rate of increase of the observed mutation trajectories as genotypes with beneficial mutations became common (see **Methods**).

This fitness trajectory fit accounts for all cells in the population, regardless of whether they have a mutation in the targeted genes or elsewhere in the genome. The red line is the maximum likelihood estimate of the population fitness trajectory. The red shading around it shows 95% confidence intervals on this value in each interval. The black line shows the increase in fitness estimated for a consensus model that was jointly fit to all mutations tracked in all six populations for which sequencing data was collected in this window. The consensus population fitness trajectory was used when estimating the fitness effects of individual mutations (see **Methods**)

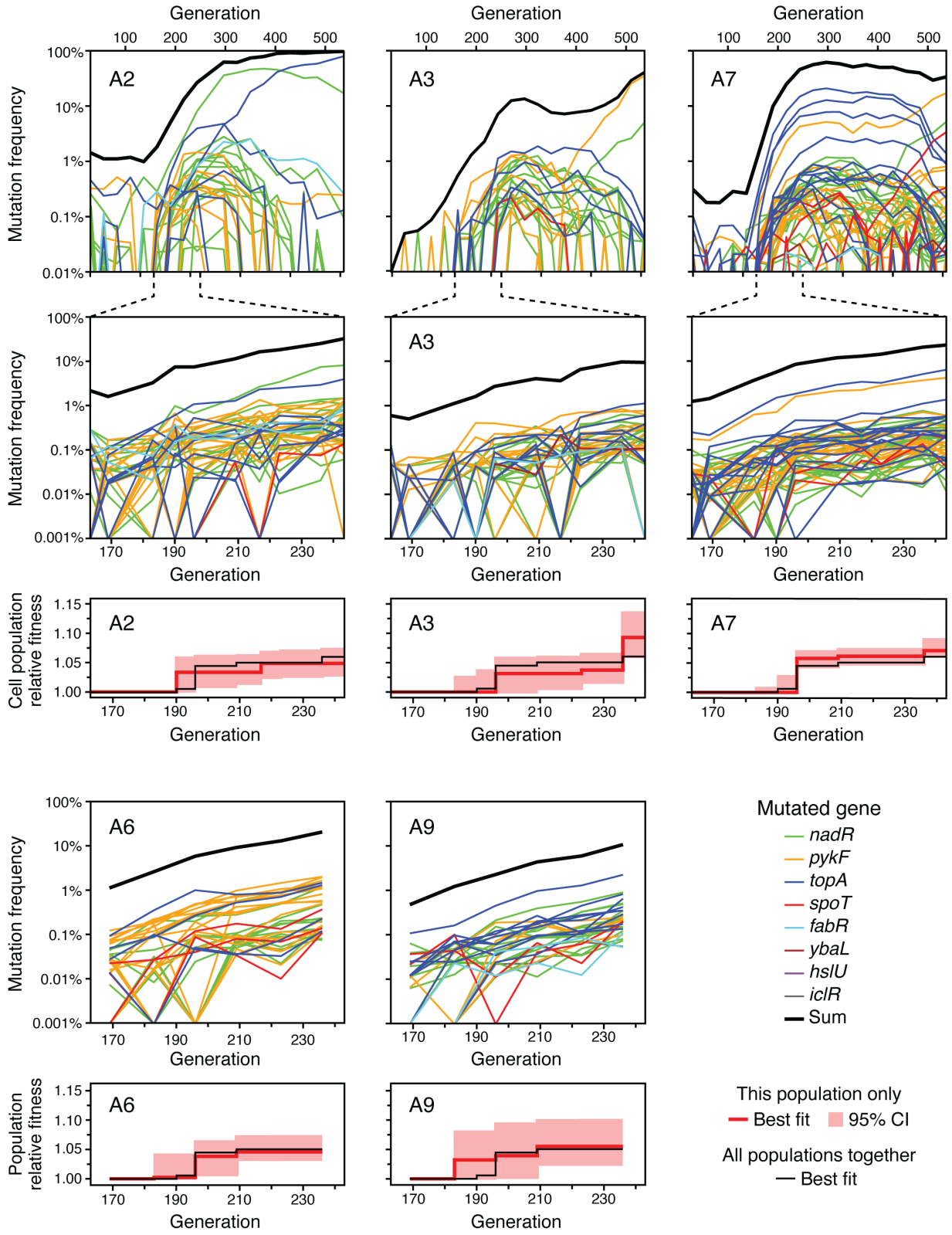
Generation
100
200
300
400
500
A2
A3
A7
Mutation frequency
100%
10%
1%
0.1%
0.01%
0.001%
170
190
210
230
Cell population relative fitness
1.15
1.10
1.05
1.00
A6
A9
Population relative fitness
Mutated gene
nadR
pykF
topA
spoT
fabR
ybaL
hslU
iclR
Sum
This population only
Best fit
95% CI
All populations together
Best fit

181

Figure 3. Frequency trajectories of mutations in the remaining populations. The same plots described in Figure 2C-E for population A1 are shown for populations A2, A3, and A7 (top three sets of panels). For populations A6 and A9, sequencing was only performed at time points during the selective sweep window so only the plots corresponding to Figure 2D-E are shown (bottom two sets of panels).

Mutation trajectories in all four populations exhibited a burst of genetic diversity in the targeted genes followed by loss of this diversity. The initial dynamics are expected to be largely driven by new genotypes that each evolve a single beneficial mutation very early in the experiment. If their descendants escape stochastic loss, they will gradually increase in frequency over the first few hundred generations as they outcompete the ancestral genotype. Once the population becomes dominated by these first-step mutants, their frequency trajectories plateau because of clonal interference: they are now mainly competing against one another and are relatively evenly matched. In populations A1, A2, and A7, the total frequencies of the mutations we identified sums to 50-62% at generation 270, indicating that each population is mostly composed of genotypes with a single mutation in one of the focal genes. We recovered less of the initial beneficial mutation diversity in population A3 where this sum was only 13%.

After around 300 generations, there is a steady decline in the frequencies of most mutations in the eight targeted genes. At this point, new more-fit genotypes that have evolved begin to exert their influence and displace the genotypes that we initially tracked. Many of the most successful new genotypes are descended from cells that already had a mutation in one of the targeted genes. In these cases, the original mutations serve as markers for the further expansion of these subpopulations after a period during which their frequencies stagnate or decrease, but the new beneficial mutations responsible for this further increase in fitness are outside of the genomic regions we surveilled. The converse situation, in which a beneficial mutation in one of the eight focal genes appears in a cell with an untracked beneficial mutation elsewhere in the

genome, also occurs in a few cases. Most strikingly, a mutation in *pykF* that only appears after 300 generations in population A3 rapidly increases in frequency and becomes dominant, strongly suggesting that it appeared in a genetic background with a prior, unknown beneficial mutation.

Selection coefficients can be inferred from initial mutation trajectories

We next sought to calculate the fitness benefits of individual mutations by tracking how rapidly their frequencies rose early in the experiment when they were largely competing versus the ancestral genotype because all new mutations in the population were still rare. To that end, we sequenced six populations at ~13-generation increments from 133 to 213 generations (**Fig. 2D**, **Fig. 3**). We were able to track a total of 240 mutations as they gradually increased in frequency during this critical time window. In the four populations we had already sequenced (A1, A2, A3, and A7), these mutations included 120 of the 181 previously found in the complete time course data spanning 500 generations and 54 additional mutations that were not detected in the complete time course data. We also identified 66 new mutations in the window time courses of the two populations that had not been previously sequenced (A6 and A9). Of these 240 mutations, 93.3% occurred in just three of the eight targeted genes: *nadR*, *pykF*, and *topA* **(Fig. 4A)**.

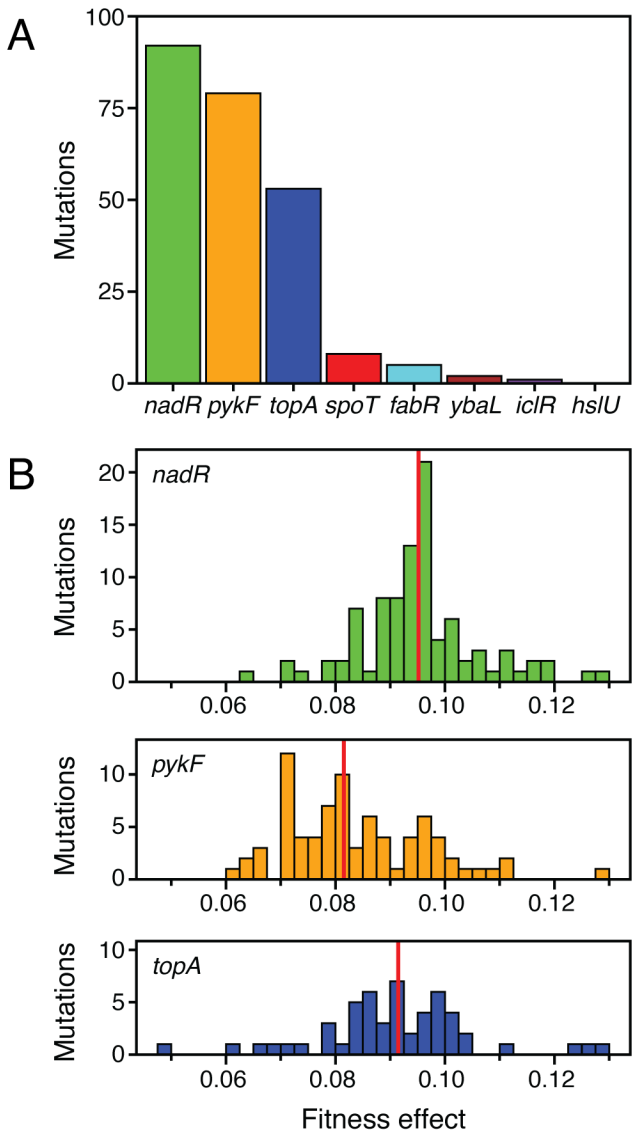

Figure 4. Characteristics of beneficial mutations in the initial selective sweep. (A) Total number of beneficial mutations in each targeted gene identified in the window time courses from 133 and 213 generations for all six profiled *E. coli* populations. (B) Distribution of selection coefficients of beneficial mutations determined from the window time courses in the three genes that were the dominant targets of selection. Vertical red lines show the mean of each distribution.

We were able to estimate the fitness effect of each of the beneficial mutations predicted in the window time courses by fitting a binomial logistic model to the counts of reads supporting the variant versus reference sequences over time. In all populations, there is initially a log-linear increase in the frequency of each mutation as the first wave of evolved cells, nearly all of which are expected to have just one of these beneficial mutations, competes against a population that is

236 still almost entirely cells with the ancestral genotype. Then, there is a deceleration in the rate at
237 which the frequencies of the new mutations increase around generation 196 that coincides with
238 the onset of clonal interference. Genotypes with beneficial mutations begin to make up a sizable
239 proportion of the population at this point, and making it necessary to account for how they are
240 increasingly competing against one another to estimate the fitness effect.

241 We accounted for clonal interference by adding a stepwise increase in the average fitness of
242 the entire cell population over time as an additional set of parameters to the binomial logistic
243 model (**Fig. 2E**, **Fig. 3**). That is, we estimated how the population fitness as a whole was
244 changing from the deceleration in the trajectories of the subset of mutations that we tracked in
245 the targeted genes. Because overall population fitness dynamics are highly reproducible from
246 population to population in the LTEE conditions (Lenski et al., 1991), we used one consensus
247 population fitness increase fit from all tracked mutations in all six sequenced populations to
248 correct our estimates of individual mutation fitness effects for clonal interference. Most of the
249 increase in population fitness occurs rapidly in a single step during the interval spanning 196-209
250 generations. This rapid change followed by stasis may seem at odds with the continuing increase
251 in the trajectories of many beneficial mutations. However, this type of stepwise increase is a
252 typical result of clonal dynamics in models and experiments (Gerrish and Lenski, 1998; Lenski
253 et al., 1991). It could reflect the influence of many mutations with small fitness effects, no one of
254 which reaches an observable frequency, peaking and then being outcompeted by the most
255 beneficial mutations that we are able to track, for example.

256 The mean fitness effect that we inferred for the 240 tracked mutations in all six populations
257 was 9.00% with a standard deviation of 1.33%. Although the distributions of the fitness effects
258 estimated for mutations in *nadR*, *pykF*, and *topA* overlap **(Fig. 4B)**, there was a significant

259 stratification among these genes. Mutations in *nadR* were 0.44% more beneficial than mutations
260 in *topA*, on average, and this difference was significant ($p = 0.022$, one-tailed Mann–Whitney U
261 test). In turn, mutations in *topA* were 0.70% more beneficial than those in *pykF* ($p = 0.00046$,
262 one-tailed Mann–Whitney U test). The fitness effects of the 16 mutations in the other genes
263 (*spoT*, *fabR, ybaL*, and *iclR*) were not significantly different from the those of the 224 mutations
264 in *nadR*, *pykF*, and *topA* ($p = 0.33$, two-tailed Mann–Whitney U test). Thus, highly beneficial
265 mutations are possible in these genes as well, but they apparently occur at a much lower rate
266 relative to that at which similarly beneficial mutations are generated in *nadR*, *pykF*, and *topA*.

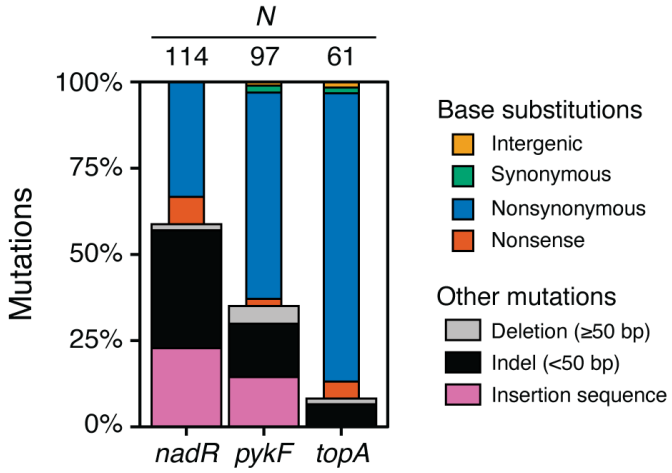

267
268
269 **Figure 5. Spectra of early beneficial mutations in *nadR*, *pykF*, and *topA*.** These three genes
270 were the dominant targets of selection during the evolution experiment among the eight genes
271 profiled for beneficial mutations. The bars include mutations identified in each of the six
272 sequenced populations in its window time course, complete time course, or both. The total
273 number of mutations identified in each gene is indicated above its column.
274

275 **Beneficial mutations reveal different signatures of selection on gene function**

276 Of the 301 mutations that we were able to track in complete or window time courses, 272 were
277 in the *nadR*, *pykF*, or *topA* genes. These large sets of highly beneficial mutations in these genes
278 gave us the statistical power to test for several signatures of molecular evolution to predict what
279 types of changes in the function of each gene improved *E. coli* fitness in this environment. Each

280 of the three genes exhibited a distinct spectrum of beneficial mutations (**Fig. 5**). In some cases,
281 different types of mutations were also unevenly distributed throughout the sequences of these
282 three commonly hit genes and had noticeably different effects on bacterial fitness (**Fig. 6A**).
283

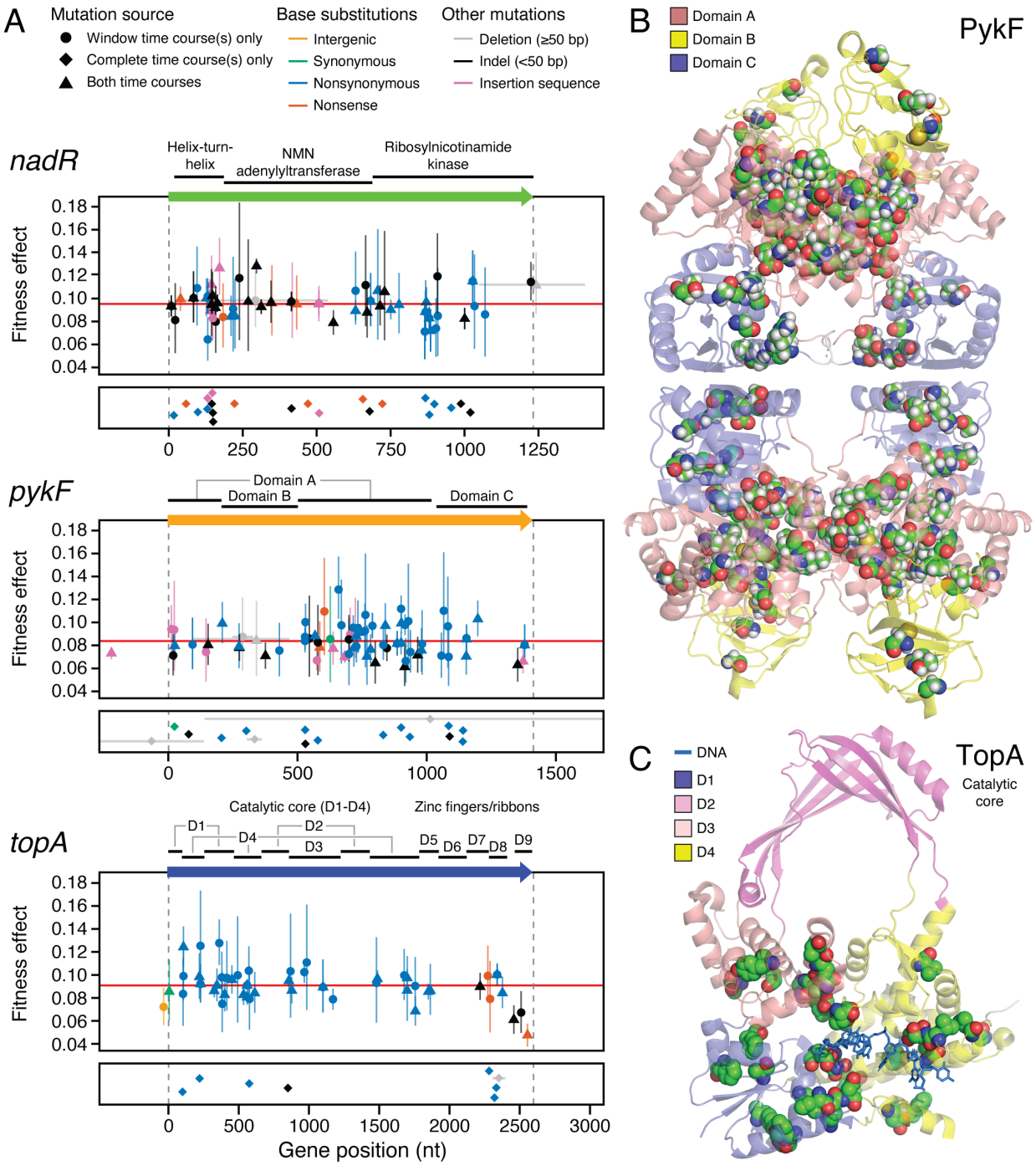

Figure 6. Mutations in the three genes that were the dominant targets of selection. (A) Nucleotide positions and properties of all mutations found in each of the three genes that were the dominant targets of selection during the evolution experiment. Colors represent the type of mutation. Symbols indicate whether each mutation was detected in the window time course, the complete time course, or both. The upper panel for each gene, shows the fitness effects estimated for mutations in that gene from the window time courses. Error bars are 95% confidence limits. When the same genetic change was detected in the window time courses for multiple populations the trajectories were combined to estimate one overall fitness value and confidence limit for all

293 of those mutations (see **Methods**). Thus, the symbols and error bars for these mutations overlap
294 in these cases. The reading frame of the gene is shown above this panel with protein domains
295 labeled. Vertical dashed grey lines represent the start and end of each gene. Horizontal grey lines
296 show the extent of large deletions within the pictured region. Horizontal red lines represent the
297 average fitness effects for all mutations in a gene. The lower panel for each gene shows
298 mutations that were only detected in the complete time courses and therefore do not have an
299 estimated fitness effect. Symbols in this panel are randomly jittered in the vertical direction to
300 improve their visibility. (B) Structural context of mutations in PykF. Sites of nonsymonymous
301 mutations are highlighted by showing space-filling models of the substituted amino acid
302 residues. All four subunits of the PykF homotetramer are shown. (C) Structural context of
303 mutations in the catalytic core of TopA. Sites of nonsymonymous mutations are highlighted by
304 showing space-filling models of the substituted amino acid residues. Only domains D1-D4 are
305 present in the structure. The DNA strand interacting with TopA is shown as a stick model.

306 The *E. coli nadR* gene has three distinct functions related to NAD biosynthesis: (1) the N-
307 terminal domain is a helix-turn-helix that binds to DNA so that it can act as a negative
308 transcriptional regulator of NAD salvage and transport pathways; (2) the internal domain is an
309 NMN adenylyltransferase (Raffaelli et al., 1999); and (3) the C-terminal domain is predicted to
310 have ribosylnicotinamide kinase activity (Kurnasov et al., 2003). Large deletions, frameshifts
311 from small insertions or deletions (indels), insertions of transposable insertion sequence (IS)
312 elements, and base substitutions creating stop codons dominate the *nadR* mutational spectrum
313 (**Fig. 5**). These disruptive mutations, which are expected to result in complete loss of gene
314 function, are significantly overrepresented versus nonsynonymous base substitutions in the first
315 two domains of the gene compared to the remainder (13.7 odds ratio, $p = 1.2 \times 10^{-8}$, one-tailed
316 Fisher's exact test) (**Fig. 6A**). Yet, there was not a significantly greater selection coefficient for
317 disruptive mutations compared to nonsynonymous mutations overall ($p = 0.063$, one-tailed
318 Mann–Whitney U test). These results suggest that complete inactivation of *nadR* yields the
319 maximum benefit possible for a mutation in this gene. Disrupting all three of its distinct
320 functions does not appear to be necessary for achieving this full benefit. Consistent with this
321 prediction, deletion of *nadR* has been shown to be highly beneficial in the very similar
322 environment of the LTEE (Barrick et al., 2009).

323 Pyruvate kinase 1 (*pykF*) catalyzes the final step of glycolysis, transferring a phosphate group
324 from phophoenolpyruvate (PEP) to ADP to generate pyruvate and ATP. It is a key enzyme in
325 regulating glycolytic flux (Kochanowski et al., 2013; Siddiquee et al., 2004). We observed an
326 intermediate representation of disruptive mutations in *pykF*, fewer than in *nadR* but more than in
327 *topA* (**Fig. 5**). Interestingly, nonsynonymous base substitutions in *pykF* tend to have a larger
328 selection coefficient than disruptive mutations ($p = 0.00031$, one-tailed Mann–Whitney U test)
329 (**Fig. 6A**). This finding is in agreement with a study of various *pykF* alleles that arose in the
330 LTEE which found that nearly all *pykF* point mutations were more beneficial than deletion of the
331 *pykF* gene, both in the ancestor and in evolved genetic backgrounds (Peng et al., 2018). PykF
332 forms a homotetramer in which each polypeptide folds into three structural domains (Donovan et
333 al., 2016; Mattevi et al., 1995). The central domain A forms the active site at the interface with
334 domain B and the binding site for the allosteric effector fructose 1,6-bisphosphate at the interface
335 with domain C. The nonsynonymous mutations that we observed are more concentrated than
336 expected in domain A versus the other structural domains based on their relative lengths in the
337 gene sequence ($p = 0.0018$ one-tailed binomial test) (**Fig. 6B**). Overall, these results suggest that
338 complete inactivation of *pykF* is highly beneficial in the environment of our evolution
339 experiment, but mutations that alter its activity—likely in ways that reduce glycolytic flux—are
340 even more so. It has been suggested that reducing *pykF* activity is beneficial in the similar
341 glucose-limited conditions of the LTEE because this allows more PEP to be diverted to power
342 import of glucose into cells via the phosphotransfer system (Woods et al., 2006).
343 DNA topoisomerase I (*topA*) relaxes negative supercoiling introduced into the chromosome
344 by replication and transcription (Massé and Drolet, 1999). The mutations we observed in *topA*
345 are almost exclusively single-base substitutions (**Fig. 5**), suggesting that modulating the activity

346 of this enzyme provides a fitness benefit. Indeed, complete loss of *topA* function is lethal to *E.*
347 *coli* without compensatory mutations in DNA gyrase (Dinardo et al., 1982; Pruss et al., 1982).
348 The structure of *E. coli* TopA consists of four N-terminal domains (D1-D4) that make up the
349 catalytic core and five C-terminal zinc finger and ribbon domains (D5-D9) (Tan et al., 2015).
350 The few out-of-frame indels and the large deletion that we observe truncate TopA within
351 domains D7-D9, which interact with single-stranded DNA and RNA polymerase but are not
352 critical for catalysis. Considering only the catalytic core, we find that nonsynonymous mutations
353 are more concentrated in domains D1 and D4 versus D2 and D3 than expected from their relative
354 sizes (p = 0.00068, one-tailed binomial test) (**Fig. 6C**). D1 and D4 together form the ssDNA
355 binding groove leading to the active site, and D1 also forms part of the active site at its interface
356 with D3 (Perry and Mondragón, 2003). Several base substitutions in *topA* have been shown to
357 increase positive supercoiling in evolved LTEE strains (Crozat et al., 2005, 2010). The exact
358 reason that this change in supercoiling is beneficial is unknown, but it may be linked to
359 increasing the expression of ribosomal RNAs (Crozat et al., 2005), altering gene regulation
360 responses to starvation or other stresses (Crozat et al., 2010), and/or increasing the expression of
361 genes in divergently transcribed operons (Houdaigui et al., 2019).
362

363 **Recurrent beneficial mutations do not have greater fitness effects**

364 We observed many examples of exact genetic parallelism. That is, the same mutation occurred
365 and reached high frequency in different experimental populations. Each of these *E. coli*
366 populations was founded from single cells, so we can conclude that these recurrent genetic
367 changes are due to independent mutational events. We observed a total of 252 distinct genetic
368 changes across all eight profiled genes and 31 of these were found in more than one population.

369 While no single genetic change was detected in all six populations, 2, 2, 8 and 19 changes were
370 detected in 5, 4, 3, and 2 populations, respectively. Most of these were in the three genes that
371 were the main targets of selection (*nadR*, *pykF*, and *topA*), but one that occurred in three
372 populations was in *fabR*. These mutations may be recurrent because they have a higher fitness
373 benefit than other mutations, occur at a higher rate than other mutations, are more easily detected
374 in the sequencing data, or due to some combination of these factors. We had a fitness estimate
375 for each of the 31 recurrent mutations from tracking cells with that genetic change in at least one
376 of the window time courses and had 167 fitness measurements for mutations that were observed
377 in only one population. The recurrent mutations had a 0.12% greater fitness effect, on average,
378 compared to the singleton mutations, but this difference was not significant ($p = 0.25$, one-tailed
379 Mann–Whitney U test). Thus, it is unlikely that many cases of exact genetic parallelism are due
380 to these mutations being more beneficial than others in our dataset.
381

382 **Discussion**

383 We examined bacterial evolution during the initial stages of clonal competition when there is a
384 burst of beneficial genetic diversity as many new subpopulations with different mutations evolve
385 and begin to displace the ancestral genotype. We focused on eight genes known to accumulate
386 adaptive mutations in the >70,000 generation Lenski long-term evolution experiment (LTEE)
387 with *E. coli* that used nearly the same environment as our experiments. The only difference was
388 that we added four times as much of the limiting nutrient (glucose). By combining Illumina
389 sequencing using unique molecular identifiers for error correction, hybridization-based capture
390 of DNA encoding these genes, and dense temporal sampling, we were able to identify more
391 beneficial mutations and track them at much lower frequencies than is possible with standard

392 metagenomic sequencing. We detected a total of 301 mutations in the focal genes: 181 in the
393 complete time courses of four populations and 240 in the window time courses of these
394 populations and two others, with 120 mutations overlapping between the two sets.

395 By densely sampling and deeply sequencing *E. coli* populations, we were able to characterize
396 many beneficial mutations that never reach the detection limits of standard Illumina sequencing
397 before they become casualties of clonal interference. Only 13 of the 181 mutations we detected
398 in the complete time courses ever achieved a frequency of 5% or more, which can be reliably
399 distinguished from noise by standard metagenomic sequencing, and only seven were this
400 common for 100 or more generations, such that they were likely to be detected by a typical time-
401 sampling scheme. Considering both the complete and window time courses we characterized 241
402 and 42 mutations that never reached 1% or 0.1% thresholds, respectively, at any of our sampled
403 time points. Our success in recovering rare variants meant that we discovered more examples of
404 beneficial mutations in the three commonly mutated genes (*topA*, *pykF*, and *nadR*) than have
405 been reported in many prior studies of the evolution of the twelve LTEE populations through
406 60,000 generations of evolution (Barrick et al., 2009; Deatherage et al., 2015; Good et al., 2017;
407 Ostrowski et al., 2008; Tenaillon et al., 2016; Woods et al., 2006). These large sets of mutations
408 enabled us to identify distinct molecular signatures of adaptation in each protein.

409 We profiled evolution driven by mutations in eight genes known to be targets of selection in
410 the LTEE. Mutations in four of these (*topA*, *pykF*, *spoT*, and *fabR*) reach high frequencies within
411 the first 1,000 generations of the LTEE in multiple populations (Deatherage et al., 2015; Good et
412 al., 2017). Mutations in the other four (*hslU*, *nadR*, *ybaL*, and *iclR*) are also common in the
413 LTEE, but they typically occur later (often within the first 2,000 to 10,000 generations) (Good et
414 al., 2017; Tenaillon et al., 2016). Nearly all mutations in these genes in our evolution experiment

415 were in *topA*, *pykF*, and *nadR*, but we also found multiple mutations that were similarly
416 beneficial in *spoT*, *fabR*, and *ybaL*. Mutations in *nadR* were more widespread than expected in
417 our experiment and may be more likely to completely disrupt its function than beneficial alleles
418 that evolve in the LTEE (Ostrowski et al., 2008). Mutations in *spoT* and *fabR* were rarer than
419 expected from the LTEE. One possible explanation for these slight differences is the increased
420 concentration of glucose in our experiment compared to the LTEE. These minor deviations are
421 also reminiscent of how changing a different aspect of the environment (temperature) re-focuses
422 the mutations of largest benefit that succeed early onto different subsets of genes, nearly all of
423 which eventually accumulate beneficial mutations later in the LTEE environment, in related
424 evolution experiments (Deatherage et al., 2017; Tenaillon et al., 2012). Alternatively, we cannot
425 rule out that mutations with similar fitness effects are still possible in the rarely mutated genes
426 but that there are so many fewer possibilities for these mutations that they were not often
427 sampled in our evolving populations. Despite these subtle differences between the LTEE and our
428 experiment, we were still able to account for majority of the genetic variation present in three of
429 the four populations that we profiled over the entire 500 generations by analyzing evolution in
430 the eight candidate genes.
431 We also wanted to understand to what extent we gained early warning of driver mutations by
432 deeply profiling evolution in genes we expected to be under strong selection. In general, we were
433 able to begin tracking most mutations when they were above a frequency of 0.01%. This level of
434 profiling enabled us to first detect mutations an average of 69, 150, and 290 generations before
435 they surpassed frequencies of 0.1%, 1%, and 5%, respectively. Under the conditions of our
436 experiment these intervals take roughly 10, 23, and 44 days, respectively; so, even though we
437 made these predictions retrospectively, there would have been sufficient time to complete the

438 DNA isolation, library preparation, sequencing, and analysis steps quickly enough for this
439 approach to give early warning of specific genetic variants driving evolution of these
440 populations. The amount of lead time becomes disproportionately longer at higher frequencies
441 due to clonal interference between beneficial mutations. The chances and timescales of earlier
442 detection are expected to increase even more when there are ecological interactions or spatial
443 structure that further slow the takeover of new variants, as has been demonstrated and discussed
444 in other microbial evolution experiments (Baym et al., 2016; Frenkel et al., 2015; Traverse et al.,
445 2013).

446 A further prediction is that the genes in which we observe early, but unsuccessful beneficial
447 mutations will sustain mutations again and again until they are successful in a population's
448 evolutionary future. This prediction is limited by the nature of epistatic interactions. In the LTEE
449 and other microbial evolution experiments, diminishing returns epistasis dominates between
450 beneficial mutations in different genes (Chou et al., 2011; Khan et al., 2011; Kryazhimskiy et al.,
451 2014; Wei and Zhang, 2019; Wiser et al., 2013). That is, mutations in one gene that improve the
452 fitness of the ancestor tend to still be beneficial to evolved genotypes containing beneficial
453 mutations in other genes, just less so than when those other mutations are not present.
454 Subpopulations with mutations in both *nadR* and *pykF* evolve by 20,000 generations in all 12
455 LTEE populations, and cells that also contain a mutation in *topA* are found in six of the LTEE
456 populations at this point (Tenaillon et al., 2016). By this time, mutations in *ybaL* and *spoT* are
457 also found in nine and six LTEE populations, respectively. So, for five of the six genes in which
458 we detected multiple mutations in the initial burst phase, it is likely that nearly all of them would
459 have eventually accumulated beneficial mutations if we continued our experiment.

460 The other three genes (*fabR*, *iclR*, and *hslU*) likely represent other scenarios. Mutations in
461 *fabR* transiently appear within the first 2,000 generations of the LTEE (Deatherage et al., 2015).
462 They interact unfavorably with beneficial mutations in *spoT* and other genes, such that a *fabR*
463 mutation essentially precludes further adaptation by mutating the other set of genes and vice-
464 versa (Deatherage et al., 2015; Woods et al., 2011). We detected 9 mutations in *fabR*, which was
465 more than the five we observed in *ybaL*. However, we predict that *fabR* mutations are unlikely to
466 re-emerge and be successful in the future of these populations because of their negative
467 interactions with other beneficial mutations. On the other hand, we detected only a single
468 mutation in *iclR* and a single mutation in *hslU*. Of the 12 LTEE populations, 11 have sizable
469 subpopulations with mutations in *iclR* and 11 have mutations in *hslU* by 20,000 generations,
470 which makes them more common than mutations in *spoT* and *ybaL* in the long run. Therefore,
471 mutations in *iclR* and *hslU* appear to either require the presence of mutations in other genes to
472 become highly beneficial or may not be able to experience any mutations that are beneficial
473 enough to make them competitive early on in our experiment.
474 The nature of epistasis and the limits that it imposes on predicting the future evolution of a
475 cell population could be further probed using our approach in several ways. One could repeat the
476 evolution experiment beginning with genotypes containing different first-step beneficial
477 mutations as starting points to more finely map the fitness landscape. One could also interrogate
478 the diverse collections of cells containing different beneficial alleles that we have evolved, by
479 taking the 150-generation populations and further evolving them under different conditions to
480 map genotype by environment effects, for example. Such experiments might also reveal latent
481 beneficial mutation in other genes (e.g., *iclR* and *hslU*) that were able to outcompete the ancestor
482 in our experiment but remained below the detection limit because they were not as beneficial as

483 mutations in *topA*, *pykF*, and *nadR* in this environment. There is precedent for changes in the
484 environment deflecting selection to different subsets of the same genes. In an offshoot of the
485 LTEE that began with a clone that had *spoT*, *topA*, and *pykF* mutations, selection was focused on
486 either *hslU*, *iclR*, or *nadR* depending on changes in temperature (Deatherage et al., 2017).
487 Alternative and complementary methods exist for deeply profiling the evolutionary
488 possibilities inherent in the fitness landscape of a cell, i.e., its evolvome. We tracked spontaneous
489 beneficial mutations within targeted genome regions, or a portion of what one could more
490 specifically describe as the adaptome (Ryall et al., 2012). Amplicon sequencing can also capture
491 mutations in a subset of the genome with deep coverage (Chubiz et al., 2012; Fischer et al.,
492 2017; Hong et al., 2018). We used hybridization-based enrichment, which did not require any
493 experimental optimization for different targets and is less likely to introduce biases in inferring
494 the frequencies of mutations when IS insertions and large indels that change amplicon sizes are
495 present. Similar procedures have been used to detect mutations associated with cancer when they
496 are only present at very low frequencies in circulating tumor DNA found in patient blood
497 samples (Newman et al., 2014, 2016). Tracking the frequencies of barcoded cells and their
498 progeny has been used to characterize the statistical properties of much larger collections of
499 naturally occurring beneficial mutations and when they are much rarer within cell populations
500 (Levy et al., 2015; Venkataram et al., 2016). However, one must barcode individuals in the
501 population to apply this method, which may be difficult in certain cell types or in clinical
502 samples, and additional genome sequencing after an experiment is completed is required to
503 discover the identities of the beneficial mutations linked to barcodes. Other methods such as
504 deep-mutational scanning (Fowler and Fields, 2014) or CRISPR-enabled trackable genome
505 engineering (Garst et al., 2017) can simultaneously interrogate large libraries of mutants to map

506 evolvomes. However, since they artificially construct variant libraries, they do not necessarily
507 provide information about which genetic variants are accessible by spontaneous mutations and
508 would therefore be expected to contribute the most to a cell's adaptome.
509 Exhaustively mapping paths that clonal evolution is likely to follow is of particular interest
510 and utility in systems that evolve repeatedly from a defined starting point. These range from
511 bioreactors that are seeded with the same strain in different production runs to lung infections in
512 cystic fibrosis patients that start from similar, but not identical, opportunistic pathogens. The
513 ability to identify mutations in key genes while they are still very rare may also be used to
514 improve the early detection of emerging drug resistance in other human infections and cancer.
515 The evolutionary dynamics will be more complex in many of these systems, but they may also
516 unfold more slowly. For example, biofilm formation and the necessity of invading already
517 colonized niches will slow the dynamics of competition. This potentially makes the therapeutic
518 window for detecting incipient evolution by profiling the adaptome even greater.
519

520 ## Materials and Methods

521 **Evolution experiment**

522 Strains and growth conditions are derived from the Lenski long-term evolution experiment
523 (Lenski and Travisano, 1994; Lenski et al., 1991). Nine colonies of *E. coli* B strain REL606 and
524 nine of strain REL607 were selected at random. Each was used to inoculate a separate flask
525 containing 10 mL of Davis Minimal (DM) media supplemented with 100 μg/L glucose
526 (DM100). This is a slightly higher concentration of glucose than the 25 μg/L glucose (DM25)
527 used in the LTEE, but still well below the ~1000 μg/L concentration at which nutrients other
528 than glucose begin to limit growth in this medium. We used this higher glucose concentration to

529 ensure we had a sufficient number of cells for sequencing and archiving. These initial cultures
530 were grown overnight at 37°C with orbital shaking over a one-inch diameter at 120 RPM.
531 Approximately 30 generations of growth occurred starting from the initial single cell that gave
532 rise to each colony until saturation of these cultures. Next, 10 mL of fresh DM100 were
533 inoculated with 50 µL of one REL606 culture and 50 µL of one REL607 culture for overnight
534 growth in the same conditions. The remaining culture was archived at −80°C with 2 mL
535 dimethyl sulfoxide (DMSO) added as cryoprotectant. Daily transfer of 100 µL of overnight
536 culture to 10 mL of fresh DM100 and archival of the remaining culture volume in the same way
537 continued through 75 daily transfers. Periodically 1 µL of culture was diluted 10,000-fold in
538 sterile saline and plated on tetrazolium arabinose (TA) agar to allow growth of ~200 colonies.
539 REL606 and REL607 differ by a mutation in an arabinose utilization gene that makes REL606
540 (Ara^{-}) colonies red and REL607 (Ara^{+}) colonies pink (Lenski et al., 1991). The ratio of red to
541 pink colonies was used to monitor these populations for selective sweeps (Hegreness and
542 Kishony, 2007; Woods et al., 2011).
543
544 **DNA isolation and library preparation**
545 Genomic DNA (gDNA) was isolated from frozen population samples by first thawing each 15
546 mL conical tube on ice. Of the ~12 mL total volume of culture plus cryoprotectant, 1.2 mL was
547 transferred to a 2 mL cryovial and refrozen. The remaining ~10.8 mL was centrifuged at 6,500 ×
548 g at 4°C for 15 minutes. The resulting cell pellets were transferred with a volume of remaining
549 solution to 1.7 mL Eppendorf tubes. Then, gDNA was isolated using the PureLink Genomic
550 DNA Mini kit (Life Technologies). For each sample, 1 µg of gDNA was randomly fragmented
551 on a Covaris S2 focused-ultrasonicator.

552 Illumina libraries were constructed using the Kappa Biosystems LTP Library Preparation Kit
553 with the following modifications. End-repaired, fragmented DNA was T-tailed (rather than A-
554 tailed) in a 50 µl reaction including 10 mM dTTP and 5 units of Klenow fragment, exo^{-} (New
555 England Biolabs). Illumina adapters containing 12-base unique molecular identifiers were ligated
556 to the T-tailed fragments as previously described (Schmitt et al., 2012), except full-length
557 adapter sequences containing unique external sample barcodes were directly ligated to the T-
558 tailed dsDNA inserts to reduce the risk of cross-contamination between samples. The full list of
559 DNA sequence adaptors used is provided in **Table S1**.
560

561 **Probe design and target capture**

562 Oligonucleotide probes consisting of 60-base xGen Lockdown probes (Integrated DNA
563 Technologies) were designed to tile across each of the eight genes of interest including upstream
564 promoter elements. Probes for each gene were compared to the entire *E. coli* B strain REL606
565 reference genome (GenBank: NC_012967.1) (Jeong et al., 2009) using BLASTN (Camacho et
566 al., 2009). The starting positions of all probes in a set were shifted by one base at a time until
567 every probe had only a single significant predicted binding location (match with E-value <
568 2×10^{-5}). The sequences of the final set of 242 probes are provided in **Table S2**.
569 Capture was performed using a SeqCap EZ Exome Enrichment kit v3.0 (NimbleGen) with
570 several modifications to the protocol. First, 18 to 20 population samples with different sample
571 barcodes were pooled together in a single capture reaction that contained a total of 1 µg of
572 library DNA from all samples, 1 mmol of a universal blocking oligo, and 1 mmol of a degenerate
573 sample barcode blocking oligo. The sequences of these blocking oligos are provided in **Table**
574 **S3**. Second, after hybridization for 72 h, DNA fragments hybridized to the biotinylated probes

575 were recovered using MyOne Streptavidin C1 Dynabeads (Life Technologies). Third, a final 8-
576 cycle PCR step was performed with HiFi Hotstart DNA Polymerase (Kappa Biosystems).
577
578 **Sequencing and read processing**
579 Paired-end 101- or 125-base sequencing of the final libraries was performed on an Illumina
580 HiSeq 2000 at the University of Texas at Austin the Genome Sequencing and Analysis Facility
581 (GSAF). Read sequences have been deposited into the NCBI Sequence Read Archive
582 (PRJNA601748). Raw reads were used to generate Consensus Sequence Reads (CSR) using
583 custom Python scripts that carried out the following steps. First, the beginning of each read was
584 evaluated for the presence of the expected 5′-end tag, consisting of a random 12-base unique
585 molecular identifier (UMI) followed by four fixed bases (5′-N_{12}CAGT). Read pairs lacking the
586 correct 5′-end tag on either read were discarded. Across all samples, 80.2% of read pairs had
587 both UMIs. For remaining read pairs, the UMIs found on each end were concatenated to create a
588 24-base dual-UMI that uniquely identifies the original DNA fragment that was amplified and
589 sequenced. To group all reads corresponding to the same initial DNA molecule, a FASTA file of
590 all dual-UMIs was used as input into the *ustacks* program from the Stacks software pipeline
591 (Version 1.48) (Catchen et al., 2013) with the following options: a single read was sufficient to
592 seed a stack, a single mismatch within the dual-UMI was allowed in assigning a read to a stack,
593 secondary reads and haplotypes were disabled, and stacks with high coverage were preserved.
594 Then, CSRs were generated for all dual-UMI groups sequenced at least twice by taking the
595 straight consensus of all reads that were merged into that stack. If no base exceeded 50%
596 frequency at a given position in this set of reads, then that base was set as unknown (N). Of the
597 read pairs with valid dual-UMIs, 41.6% were incorporated into consensus reads across all

598 samples. The average number of dual-UMI read pairs utilized to create each consensus read was
599 2.46, which gives an overall yield of consensus reads per read in a pair with a valid dual-UMI
600 16.9%.
601
602 **Variant calling**
603 We used the *breseq* pipeline (Barrick et al., 2014; Deatherage and Barrick, 2014; Deatherage et
604 al., 2015) (version 0.26.0) to call single-nucleotide variants (SNVs) and structural variants (SVs)
605 from the CSRs. We divided the genome sequence of the ancestral *E. coli* REL606 strain into two
606 types of reference regions for mapping in this analysis. The eight regions of the genome tiled
607 with probes—extended with hundreds of bases of flanking sequence on both sides—were input
608 as "targeted" sequences, and the remainder of the genome with the identical eight regions
609 masked to degenerate N bases was supplied as a "junction-only" reference (to which reads are
610 mapped without variant calling). All 116 samples were analyzed using *breseq* in polymorphism
611 prediction mode with all bias, minimum allele frequency, and read-count filters disabled.
612 Evidence items in the Genome Diff (GD) files for all samples were combined using the *gdtools*
613 utility program to generate a single merged GD file with each piece of evidence listed a single
614 time, regardless of how many times it was detected in different samples. We then re-ran *breseq*
615 using the same parameters except that this GD file was supplied as an input user-evidence file to
616 force output of variant and reference information for these putative variants in every sample.
617 Then, we extracted the number of variant reads supporting each putative variant allele and the
618 total number of reads at that reference location from the GD file output by *breseq*. Subsequent
619 statistical tests and fitting steps were performed in R (version 4.0.0) (R Core Team, 2016) using

620 the ggplot2 package for data visualization (Wickham, 2016). Scripts and data files for this
621 analysis are available in GitHub (https://github.com/barricklab/adaptome-capture).
622 Since this original analysis was conducted at the level of *breseq* evidence (i.e., single
623 columns of read pileups on the reference genome or instances of new sequence junctions), we
624 next merged sets of observations that were consistent with a single mutational event when they
625 also had frequency trajectories that tracked together. To identify these candidates for merging,
626 we analyzed each of the six window (generation 133 to 213) and four complete (generation 0 to
627 500) time courses separately. We only considered mutations that exceeded a threshold frequency
628 of 0.03% at some time during each time course as candidates for merging.
629 Read alignment (RA) evidence items were merged when they were located within 6 base
630 pairs of one another and within a normalized Canberra distance of 0.1 between the vectors of
631 their frequency observations across all of the time points in a dataset. All RA evidence pairs of
632 this kind were found to co-occur in the same sequencing reads. For these cases, the read counts
633 for the first linked mutation were used to represent the entire event. For example, if a deletion of
634 three base pairs was predicted by missing bases at positions x, y, and z; then the frequency of
635 missing the first base (x) was assigned to the entire three-base deletion mutation.
636 For new junction (JC) evidence we performed the same merging procedure but allowed
637 linked mutations to be within a larger window of 20 base pairs and within a normalized Canberra
638 distance of 0.5. JC pairs passing these criteria were only merged if they were also consistent with
639 an IS-element insertion in terms of their relative orientation and spacing. In this case the variant
640 and total read counts were added together for the two different junctions, as the junctions on each
641 side of the inserted IS element provide independent information for estimating the frequency of
642 this type of mutation. We allowed unpaired JC evidence passing the filters to also predict IS

643 element mutations. This situation may indicate that there was an IS-mediated deletion between
644 an element that inserted within the gene and another element from the same family located
645 outside of the targeted region or more complex chromosomal rearrangements involving a newly
646 inserted IS element (Raeside et al., 2014).
647
648 **Time course filtering and fitness effect estimation**
649 After merging evidence of genetic variants into lists of putative mutations, we further eliminated
650 some of these from consideration using several filtering steps. For the complete time courses, we
651 first required that non-zero frequencies be observed for a mutation in samples from at least two
652 different time points. We next applied a filter to eliminate spurious variants that can be
653 recognized as arising from systematic sequencing or alignment errors because they do not exhibit
654 the correlated changes in frequency over time expected for the frequency trajectories of real
655 mutations (Lang et al., 2013). Specifically, we required that the time-series of estimated
656 frequencies for a mutation over all analyzed time points have an autocorrelation value ≥ 0.55.
657 For the window time courses, we eliminated putative mutations for which there was great
658 uncertainty in the estimated fitness effect or evidence that its trajectory reflected multiple
659 beneficial mutations occurring in the same genome. Specifically, we required that a mutation
660 was first observed at generation 196 or earlier and that its estimated frequency was $\geq 10^{-4}$ in
661 every sample that was sequenced from generation 223 to 243. Then, we fit a binomial logistic
662 model with slope and *y*-intercept terms to the time courses of counts of variant and reference
663 (total minus variant) observations for each mutation. We used a negative offset in the model of
664 the number of generations up to each time point so that the slope represents one plus the
665 selection coefficient that is characteristic of the subpopulation with that mutation. We filtered out

666 any mutations for which this fit had an AIC < 200, a *p*-value for the slope differing from zero of
667 > 0.005, or a *y*-intercept < –20. The fitness effects that we report for mutations are the selection
668 coefficients fit from the model divided by the natural logarithm of two so that they are expressed
669 per generations of binary cell division. One plus the fitness effect is the relative fitness of a cell
670 with that mutation. These values can be directly compared to experimental measurements of
671 relative fitness and mutation fitness effects made using co-culture competition assays (Lenski et
672 al., 1991; Tenaillon et al., 2016).

673 This procedure for determining fitness effects assumes that the trajectories reflect
674 competition purely against the ancestral strain. However, we detected a consistent deviation from
675 linearity for all mutation trajectories in the window time courses after generation 196. The rates
676 at which the frequencies of all mutations were increasing decelerated, indicating that the overall
677 population fitness had improved to a degree that it reduced their effective advantage versus their
678 competitors. To account for this change we fit additional parameters defining a stepwise increase
679 in the average relative fitness of the population within each interval between sequenced samples
680 from generation 196 onward. The increase in population fitness reduces the effective time basis
681 used in the model to determine the slope to the number of generations in each interval divided by
682 the average relative fitness during that interval. We determined the population fitness values that
683 minimized the AIC of this modified binomial logistic model. The figures show the best stepwise
684 increases in population fitness between the sequenced time points from generation 196 onward
685 fitting to the trajectories of all mutations in a given population at the same time. We performed
686 1000 bootstrap resamplings of the mutations in each population to estimate 95% confidence
687 intervals on the estimated population fitness values in each interval for that population.

688 We combined information across multiple populations in two ways to further improve the
689 estimates of mutation fitness effects. First, there was considerable uncertainty in the estimates of
690 the stepwise population fitness increases for each population considered alone. Because the
691 actual population fitness trajectories of all populations are expected to be highly similar to one
692 another, we fit a consensus stepwise increase in population fitness over time that best improved
693 the fits for all mutations from all populations. Second, we observed 27 cases in which the exact
694 same change in a gene's sequence was observed and passed our filtering criteria in the window
695 time courses of multiple experimental populations. Because each population was started from
696 single cells, we can be sure that these are independent observations of the same mutation.
697 Therefore, we fit one consensus fitness effect (slope) for each of these recurrent mutations across
698 all populations. We still allowed the *y*-intercept for each of these mutations to vary from
699 population to population because this parameter is related to how early the mutation evolved,
700 which is expected to be different in each replicate population.
701
702 **Protein structure analysis**
703 Structural domains in NadR, PykF, and TopA were defined according to UniProt and papers
704 reporting x-ray crystal structures. Mutations in PykF were mapped onto Protein Data Bank
705 structure 4YNG (Donovan et al., 2016). Mutations in TopA were mapped onto Protein Data
706 Bank structure 1MW8 (Perry and Mondragón, 2003). Protein structures were visualized using
707 Pymol v2.3.5 (Schrödinger LLC).
708
709 **Acknowledgements**

The authors acknowledge the Texas Advanced Computing Center (TACC) at The University of Texas at Austin for providing high-performance computing resources.

Supporting Information

Table S1 Adapter sequences used in DNA library preparation

Table S2 Sequences of pulldown probes

Table S3 Blocking oligos used to limit read-to-read binding during pulldown

Author contributions

Conceptualization: DED JEB.

Data Curation: DED JEB.

Funding Acquisition: DED JEB.

Investigation: DED.

Methodology: DED JEB.

Software – DED JEB.

Supervision – JEB.

Visualization: DED JEB.

Writing – Original Draft Preparation: DED JEB.

Writing – Review & Editing: DED JEB.

References

Bainbridge, M.N., Wang, M., Burgess, D.L., Kovar, C., Rodesch, M.J., D'Ascenzo, M., Kitzman, J., Wu, Y.-Q., Newsham, I., Richmond, T. a, et al. (2010). Whole exome capture in solution with 3 Gbp of data. Genome Biol. *11*, R62.

Barrick, J.E. (2020). Limits to predicting evolution: insights from a long-term experiment with

736 *Escherichia coli*. In Evolution in Action: Past, Present and Future, W. Banzhaf, B.H.C. Cheng,
737 K. Deb, K.E. Holekamp, R.E. Lenski, C. Ofria, R.T. Pennock, W.F. Punch, and D.J. Whittaker,
738 eds. (Cham: Springer), pp. 63–76.

739 Barrick, J.E., and Lenski, R.E. (2009). Genome-wide mutational diversity in an evolving
740 population of *Escherichia coli*. Cold Spring Harb. Symp. Quant. Biol. *74*, 119–129.

741 Barrick, J.E., and Lenski, R.E. (2013). Genome dynamics during experimental evolution. Nat.
742 Rev. Genet. *14*, 827–839.

743 Barrick, J.E., Yu, D.S., Yoon, S.H., Jeong, H., Oh, T.K., Schneider, D., Lenski, R.E., and Kim,
744 J.F. (2009). Genome evolution and adaptation in a long-term experiment with *Escherichia coli*.
745 Nature *461*, 1243–1247.

746 Barrick, J.E., Colburn, G., Deatherage, D.E., Traverse, C.C., Strand, M.D., Borges, J.J.,
747 Knoester, D.B., Reba, A., and Meyer, A.G. (2014). Identifying structural variation in haploid
748 microbial genomes from short-read resequencing data using *breseq*. BMC Genomics *15*, 1039.

749 Baym, M., Lieberman, T.D., Kelsic, E.D., Chait, R., Gross, R., Yelin, I., and Kishony, R. (2016).
750 Spatiotemporal microbial evolution on antibiotic landscapes. Science *353*, 1147–1151.

751 Camacho, C., Coulouris, G., Avagyan, V., Ma, N., Papadopoulos, J., Bealer, K., and Madden,
752 T.L. (2009). BLAST+: architecture and applications. BMC Bioinformatics *10*, 421.

753 Catchen, J., Hohenlohe, P.A., Bassham, S., Amores, A., and Cresko, W.A. (2013). Stacks: an
754 analysis tool set for population genomics. Mol. Ecol. *22*, 3124–3140.

755 Chou, H.-H., Chiu, H.-C., Delaney, N.F., Segrè, D., and Marx, C.J. (2011). Diminishing returns
756 epistasis among beneficial mutations decelerates adaptation. Science *332*, 1190–1192.

757 Chubiz, L.M., Lee, M.-C., Delaney, N.F., and Marx, C.J. (2012). FREQ-Seq: a rapid, cost-
758 effective, sequencing-based method to determine allele frequencies directly from mixed
759 populations. PLoS ONE *7*, e47959.

760 Crozat, E., Philippe, N., Lenski, R.E., Geiselmann, J., and Schneider, D. (2005). Long-term
761 experimental evolution in *Escherichia coli*. XII. DNA topology as a key target of selection.
762 Genetics *169*, 523–532.

763 Crozat, E., Winkworth, C., Gaffé, J., Hallin, P.F., Riley, M.A., Lenski, R.E., and Schneider, D.
764 (2010). Parallel genetic and phenotypic evolution of DNA superhelicity in experimental
765 populations of *Escherichia coli*. Mol. Biol. Evol. *27*, 2113–2128.

766 Cvijović, I., Nguyen Ba, A.N., and Desai, M.M. (2018). Experimental studies of evolutionary
767 dynamics in microbes. Trends Genet. *34*, 693–703.

768 Deatherage, D.E., and Barrick, J.E. (2014). Identification of mutations in laboratory-evolved
769 microbes from next-generation sequencing data using *breseq*. Methods Mol. Biol. *1151*, 165–
770 188.

771 Deatherage, D.E., Traverse, C.C., Wolf, L.N., and Barrick, J.E. (2015). Detecting rare structural
772 variation in evolving microbial populations from new sequence junctions using *breseq*. Front.
773 Genet. *5*, 468.

774 Deatherage, D.E., Kepner, J.L., Bennett, A.F., Lenski, R.E., and Barrick, J.E. (2017). Specificity

775 of genome evolution in experimental populations of *Escherichia coli* evolved at different
776 temperatures. Proc. Natl. Acad. Sci. U. S. A. *114*, E1904–E1912.

777 Desai, M.M., Walczak, A.M., and Fisher, D.S. (2012). Genetic diversity and the structure of
778 genealogies in rapidly adapting populations. Genetics *193*, 565–585.

779 Dinardo, S., Voelkel, K.A., Sternglanz, R., Reynolds, A.E., and Wright, A. (1982). *Escherichia*
780 *coli* DNA topoisomerase I mutants have compensatory mutations in DNA gyrase genes. Cell *31*,
781 43–51.

782 Ding, L., Ley, T.J., Larson, D.E., Miller, C. a., Koboldt, D.C., Welch, J.S., Ritchey, J.K., Young,
783 M. a., Lamprecht, T., McLellan, M.D., et al. (2012). Clonal evolution in relapsed acute myeloid
784 leukaemia revealed by whole-genome sequencing. Nature *481*, 506–510.

785 Donovan, K.A., Atkinson, S.C., Kessans, S.A., Peng, F., Cooper, T.F., Griffin, M.D.W.,
786 Jameson, G.B., and Dobson, R.C.J. (2016). Grappling with anisotropic data, pseudo-merohedral
787 twinning and pseudo-translational noncrystallographic symmetry: A case study involving
788 pyruvate kinase. Acta Crystallogr. Sect. D Struct. Biol. *72*, 512–519.

789 Fischer, S., Greipel, L., Klockgether, J., Dorda, M., Wiehlmann, L., Cramer, N., and Tümmler,
790 B. (2017). Multilocus amplicon sequencing of *Pseudomonas aeruginosa* cystic fibrosis airways
791 isolates collected prior to and after early antipseudomonal chemotherapy. J. Cyst. Fibros. *16*,
792 346–352.

793 Fowler, D.M., and Fields, S. (2014). Deep mutational scanning: a new style of protein science.
794 Nat. Methods *11*, 801–807.

795 Frenkel, E.M., McDonald, M.J., Van Dyken, J.D., Kosheleva, K., Lang, G.I., and Desai, M.M.
796 (2015). Crowded growth leads to the spontaneous evolution of semistable coexistence in
797 laboratory yeast populations. Proc. Natl. Acad. Sci. *112*, 11306–11311.

798 Furusawa, C., Horinouchi, T., and Maeda, T. (2018). Toward prediction and control of
799 antibiotic-resistance evolution. Curr. Opin. Biotechnol. *54*, 45–49.

800 Garst, A.D., Bassalo, M.C., Pines, G., Lynch, S.A., Halweg-Edwards, A.L., Liu, R., Liang, L.,
801 Wang, Z., Zeitoun, R., Alexander, W.G., et al. (2017). Genome-wide mapping of mutations at
802 single-nucleotide resolution for protein, metabolic and genome engineering. Nat. Biotechnol. *35*,
803 48–55.

804 Genovese, G., Kähler, A.K., Handsaker, R.E., Lindberg, J., Rose, S.A., Bakhoum, S.F.,
805 Chambert, K., Mick, E., Neale, B.M., Fromer, M., et al. (2014). Clonal hematopoiesis and blood-
806 cancer risk inferred from blood DNA sequence. N. Engl. J. Med. *371*, 2477–2487.

807 Gerrish, P.J., and Lenski, R.E. (1998). The fate of competing beneficial mutations in an asexual
808 population. Genetica *102–103*, 127–144.

809 Good, B.H., McDonald, M.J., Barrick, J.E., Lenski, R.E., and Desai, M.M. (2017). The dynamics
810 of molecular evolution over 60,000 generations. Nature *551*, 45–50.

811 Gresham, D., and Dunham, M.J. (2014). The enduring utility of continuous culturing in
812 experimental evolution. Genomics *104*, 399–405.

813 Hegreness, M., and Kishony, R. (2007). Analysis of genetic systems using experimental

814 evolution and whole-genome sequencing. Genome Biol. *8*, 201.

815 Hegreness, M., Shoresh, N., Hartl, D., and Kishony, R. (2006). An equivalence principle for the
816 incorporation of favorable mutations in asexual populations. Science *311*, 1615–1617.

817 Hong, J., Brandt, N., Abdul-Rahman, F., Yang, A., Hughes, T., and Gresham, D. (2018). An
818 incoherent feedforward loop facilitates adaptive tuning of gene expression. Elife *7*, 1–18.

819 Houdaigui, B. El, Forquet, R., Hindré, T., Schneider, D., Nasser, W., Reverchon, S., and Meyer,
820 S. (2019). Bacterial genome architecture shapes global transcriptional regulation by DNA
821 supercoiling. Nucleic Acids Res. *47*, 5648–5657.

822 Jeong, H., Barbe, V., Lee, C.H., Vallenet, D., Yu, D.S., Choi, S.-H., Couloux, A., Lee, S.-W.,
823 Yoon, S.H., Cattolico, L., et al. (2009). Genome sequences of *Escherichia coli* B strains REL606
824 and BL21(DE3). J. Mol. Biol. *394*, 644–652.

825 Khan, A.I., Dinh, D.M., Schneider, D., Lenski, R.E., and Cooper, T.F. (2011). Negative epistasis
826 between beneficial mutations in an evolving bacterial population. Science *332*, 1193–1196.

827 Kochanowski, K., Volkmer, B., Gerosa, L., Van Rijsewijk, B.R.H., Schmidt, A., and
828 Heinemann, M. (2013). Functioning of a metabolic flux sensor in *Escherichia coli*. Proc. Natl.
829 Acad. Sci. U. S. A. *110*, 1130–1135.

830 Kryazhimskiy, S., Rice, D.P., Jerison, E.R., and Desai, M.M. (2014). Global epistasis makes
831 adaptation predictable despite sequence-level stochasticity. Science *344*, 1519–1522.

832 Kurnasov, O. V., Polanuyer, B.M., Ananta, S., Sloutsky, R., Tam, A., Gerdes, S.Y., and
833 Osterman, A.L. (2003). Ribosylnicotinamide Kinase Domain of NadR Protein: Identification and
834 Implications in NAD Biosynthesis. J. Bacteriol. *185*, 698–698.

835 Landau, D.A., Carter, S.L., Stojanov, P., McKenna, A., Stevenson, K., Lawrence, M.S.,
836 Sougnez, C., Stewart, C., Sivachenko, A., Wang, L., et al. (2013). Evolution and impact of
837 subclonal mutations in chronic lymphocytic leukemia. Cell *152*, 714–726.

838 Lang, G.I., Rice, D.P., Hickman, M.J., Sodergren, E., Weinstock, G.M., Botstein, D., and Desai,
839 M.M. (2013). Pervasive genetic hitchhiking and clonal interference in forty evolving yeast
840 populations. Nature *500*, 571–574.

841 Lee, S.Y., and Kim, H.U. (2015). Systems strategies for developing industrial microbial strains.
842 Nat. Biotechnol. *33*, 1061–1072.

843 Lenski, R.E., and Travisano, M. (1994). Dynamics of adaptation and diversification: a 10,000-
844 generation experiment with bacterial populations. Proc. Natl. Acad. Sci. U. S. A. *91*, 6808–6814.

845 Lenski, R.E., Rose, M.R., Simpson, S.C., and Tadler, S.C. (1991). Long-term experimental
846 evolution in *Escherichia coli*. I. Adaptation and divergence during 2,000 generations. Am. Nat.
847 *138*, 1315–1341.

848 Levy, S.F., Blundell, J.R., Venkataram, S., Petrov, D.A., Fisher, D.S., and Sherlock, G. (2015).
849 Quantitative evolutionary dynamics using high-resolution lineage tracking. Nature *519*, 181–186.

850 Maddamsetti, R., Lenski, R.E., and Barrick, J.E. (2015). Adaptation, clonal interference, and
851 frequency-dependent interactions in a long-term evolution experiment with *Escherichia coli*.
852 Genetics *200*, 619–631.

853 Marusyk, A., Almendro, V., and Polyak, K. (2012). Intra-tumour heterogeneity: A looking glass
854 for cancer? Nat. Rev. Cancer *12*, 323–334.

855 Marvig, R.L., Sommer, L.M., Molin, S., and Johansen, H.K. (2015). Convergent evolution and
856 adaptation of *Pseudomonas aeruginosa* within patients with cystic fibrosis. Nat. Genet. *47*, 57–
857 64.

858 Massé, E., and Drolet, M. (1999). Relaxation of transcription-induced negative supercoiling is an
859 essential function of *Escherichia coli* DNA topoisomerase I. J. Biol. Chem. *274*, 16654–16658.

860 Mattevi, A., Valentini, G., Rizzi, M., Speranza, M.L., Bolognesi, M., and Coda, A. (1995).
861 Crystal structure of *Escherichia coli* pyruvate kinase type I: molecular basis of the allosteric
862 transition. Structure *3*, 729–741.

863 McDonald, M.J. (2019). Microbial experimental evolution – a proving ground for evolutionary
864 theory and a tool for discovery. EMBO Rep. *20*, 1–14.

865 Merlo, L.M.F., Pepper, J.W., Reid, B.J., and Maley, C.C. (2006). Cancer as an evolutionary and
866 ecological process. Nat. Rev. Cancer *6*, 924–935.

867 Merlo, L.M.F., Shah, N.A., Li, X., Blount, P.L., Vaughan, T.L., Reid, B.J., and Maley, C.C.
868 (2010). A comprehensive survey of clonal diversity measures in Barrett's esophagus as
869 biomarkers of progression to esophageal adenocarcinoma. Cancer Prev. Res. (Phila). *3*, 1388–
870 1397.

871 Newman, A.M., Bratman, S. V., To, J., Wynne, J.F., Eclov, N.C.W., Modlin, L.A., Liu, C.L.,
872 Neal, J.W., Wakelee, H.A., Merritt, R.E., et al. (2014). An ultrasensitive method for quantitating
873 circulating tumor DNA with broad patient coverage. Nat. Med. *20*, 548–554.

874 Newman, A.M., Lovejoy, A.F., Klass, D.M., Kurtz, D.M., Chabon, J.J., Scherer, F., Stehr, H.,
875 Liu, C.L., Bratman, S. V., Say, C., et al. (2016). Integrated digital error suppression for improved
876 detection of circulating tumor DNA. Nat. Biotechnol. *34*, 547–555.

877 Nielsen, J., and Keasling, J.D. (2016). Engineering cellular metabolism. Cell *164*, 1185–1197.

878 Ostrowski, E.A., Woods, R.J., and Lenski, R.E. (2008). The genetic basis of parallel and
879 divergent phenotypic responses in evolving populations of *Escherichia coli*. Proc. R. Soc. B *275*,
880 277–284.

881 Park, S.-C., and Krug, J. (2007). Clonal interference in large populations. Proc. Natl. Acad. Sci.
882 U. S. A. *104*, 18135–18140.

883 Peng, F., Widmann, S., Wünsche, A., Duan, K., Donovan, K.A., Dobson, R.C.J., Lenski, R.E.,
884 and Cooper, T.F. (2018). Effects of beneficial mutations in *pykF* gene vary over time and across
885 replicate populations in a long-term experiment with bacteria. Mol. Biol. Evol. *35*, 202–210.

886 Perry, K., and Mondragón, A. (2003). Structure of a complex between *E. coli* DNA
887 topoisomerase I and single-stranded DNA. Structure *11*, 1349–1358.

888 Pruss, G.J., Manes, S.H., and Drlica, K. (1982). *Escherichia coli* DNA topoisomerase I mutants:
889 Increased supercoiling is corrected by mutations near gyrase genes. Cell *31*, 35–42.

890 R Core Team (2016). R: A Language and Environment for Statistical Computing (Vienna,
891 Austria: R Foundation for Statistical Computing).

892 Raeside, C., Gaffé, J., Deatherage, D.E., Tenaillon, O., Briska, A.M., Ptashkin, R.N., Cruveiller,
893 S., Médigue, C., Lenski, R.E., Barrick, J.E., et al. (2014). Large chromosomal rearrangements
894 during a long-term evolution experiment with *Escherichia coli*. MBio *5*, e01377-14.

895 Raffaelli, N., Lorenzi, T., Mariani, P.L., Emanuelli, M., Amici, A., Ruggieri, S., and Magni, G.
896 (1999). The *Escherichia coli* NadR regulator is endowed with nicotinamide mononucleotide
897 adenylyltransferase activity. J. Bacteriol. *181*, 5509–5511.

898 Rainey, P.B., Remigi, P., Farr, A.D., and Lind, P.A. (2017). Darwin was right: where now for
899 experimental evolution? Curr. Opin. Genet. Dev. *47*, 102–109.

900 Renda, B.A., Hammerling, M.J., and Barrick, J.E. (2014). Engineering reduced evolutionary
901 potential for synthetic biology. Mol. Biosyst. *10*, 1668–1678.

902 Rugbjerg, P., and Sommer, M.O.A. (2019). Overcoming genetic heterogeneity in industrial
903 fermentations. Nat. Biotechnol. *37*, 869–876.

904 Rugbjerg, P., Myling-Petersen, N., Porse, A., Sarup-Lytzen, K., and Sommer, M.O.A. (2018).
905 Diverse genetic error modes constrain large-scale bio-based production. Nat. Commun. *9*, 787.

906 Ryall, B., Eydallin, G., and Ferenci, T. (2012). Culture history and population heterogeneity as
907 determinants of bacterial adaptation: the adaptomics of a single environmental transition.
908 Microbiol. Mol. Biol. Rev. *76*, 597–625.

909 Sandoval, C.M., Ayson, M., Moss, N., Lieu, B., Jackson, P., Gaucher, S.P., Horning, T., Dahl,
910 R.H., Denery, J.R., Abbott, D.A., et al. (2014). Use of pantothenate as a metabolic switch
911 increases the genetic stability of farnesene producing *Saccharomyces cerevisiae*. Metab. Eng. *25*,
912 215–226.

913 Schmitt, M.W., Kennedy, S.R., Salk, J.J., Fox, E.J., Hiatt, J.B., and Loeb, L.A. (2012). Detection
914 of ultra-rare mutations by next-generation sequencing. Proc. Natl. Acad. Sci. U. S. A. *109*,
915 14508–14513.

916 Siddiquee, K.A.Z., Arauzo-Bravo, M.J., and Shimizu, K. (2004). Effect of a pyruvate kinase
917 (*pykF*-gene) knockout mutation on the control of gene expression and metabolic fluxes in
918 *Escherichia coli*. FEMS Microbiol. Lett. *235*, 25–33.

919 Stefani, S., Campana, S., Cariani, L., Carnovale, V., Colombo, C., Lleo, M.M., Iula, V.D.,
920 Minicucci, L., Morelli, P., Pizzamiglio, G., et al. (2017). Relevance of multidrug-resistant
921 *Pseudomonas aeruginosa* infections in cystic fibrosis. Int. J. Med. Microbiol. *307*, 353–362.

922 Tan, K., Zhou, Q., Cheng, B., Zhang, Z., Joachimiak, A., and Tse-Dinh, Y.C. (2015). Structural
923 basis for suppression of hypernegative DNA supercoiling by *E. coli* topoisomerase I. Nucleic
924 Acids Res. *43*, 11031–11046.

925 Tenaillon, O., Rodríguez-Verdugo, A., Gaut, R.L., McDonald, P., Bennett, A.F., Long, A.D., and
926 Gaut, B.S. (2012). The molecular diversity of adaptive convergence. Science *335*, 457–461.

927 Tenaillon, O., Barrick, J.E., Ribeck, N., Deatherage, D.E., Blanchard, J.L., Dasgupta, A., Wu,
928 G.C., Wielgoss, S., Cruveiller, S., Médigue, C., et al. (2016). Tempo and mode of genome
929 evolution in a 50,000-generation experiment. Nature *536*, 165–170.

930 Thomas, R.K., Nickerson, E., Simons, J.F., Jänne, P.A., Tengs, T., Yuza, Y., Garraway, L.A.,

931 LaFramboise, T., Lee, J.C., Shah, K., et al. (2006). Sensitive mutation detection in heterogeneous
932 cancer specimens by massively parallel picoliter reactor sequencing. Nat. Med. *12*, 852–855.

933 Traverse, C.C., Mayo-Smith, L.M., Poltak, S.R., and Cooper, V.S. (2013). Tangled bank of
934 experimentally evolved *Burkholderia* biofilms reflects selection during chronic infections. Proc.
935 Natl. Acad. Sci. U. S. A. *110*, E250–E259.

936 Venkataram, S., Dunn, B., Li, Y., Agarwala, A., Chang, J., Ebel, E.R., Geiler-Samerotte, K.,
937 Hérissant, L., Blundell, J.R., Levy, S.F., et al. (2016). Development of a comprehensive
938 genotype-to-fitness map of adaptation-driving mutations in yeast. Cell *166*, 1585-1596.E22.

939 Watson, C.J., Papula, A.L., Poon, G.Y.P., Wong, W.H., Young, A.L., Druley, T.E., Fisher, D.S.,
940 and Blundell, J.R. (2020). The evolutionary dynamics and fitness landscape of clonal
941 hematopoiesis. Science *367*, 1449–1454.

942 Wei, X., and Zhang, J. (2019). Patterns and mechanisms of diminishing returns from beneficial
943 mutations. Mol. Biol. Evol. *36*, 1008–1021.

944 Wickham, H. (2016). ggplot2: Elegant Graphics for Data Analysis (New York: Springer-Verlag).

945 Winstanley, C., O'Brien, S., and Brockhurst, M.A. (2016). *Pseudomonas aeruginosa*
946 evolutionary adaptation and diversification in cystic fibrosis chronic lung infections. Trends
947 Microbiol. *24*, 327–337.

948 Wiser, M.J., Ribeck, N., and Lenski, R.E. (2013). Long-term dynamics of adaptation in asexual
949 populations. Science *342*, 1364–1367.

950 Woods, R., Schneider, D., Winkworth, C.L., Riley, M.A., and Lenski, R.E. (2006). Tests of
951 parallel molecular evolution in a long-term experiment with *Escherichia coli*. Proc. Natl. Acad.
952 Sci. U. S. A. *103*, 9107–9712.

953 Woods, R.J., Barrick, J.E., Cooper, T.F., Shrestha, U., Kauth, M.R., and Lenski, R.E. (2011).
954 Second-order selection for evolvability in a large *Escherichia coli* population. Science *331*,
955 1433–1436.

956 Zelder, O., and Hauer, B. (2000). Environmentally directed mutations and their impact on
957 industrial biotransformation and fermentation processes. Curr. Opin. Microbiol. *3*, 248–251.